Applied Surface Science 538 (2021) 148099

Contents lists available at ScienceDirect

Applied Surface Science

journal homepage: www.elsevier.com/locate/apsusc

Chemical disorder of a-SiC layer induced in 6H-SiC by Cs and I ions co-implantation: Raman spectroscopy analysis

M.J. Madito[a,*], T.T. Hlatshwayo[b], C.B. Mtshali[a]

[a] iThemba LABS, National Research Foundation, PO Box 722, Somerset West 7129, Cape Town, South Africa
[b] Department of Physics, University of Pretoria, Private Bag X20, Pretoria 0002, South Africa

ARTICLE INFO

Keywords:
6H-SiC
Raman imaging
Cs ions
Iodine ions
Amorphous SiC
Ion implantation

ABSTRACT

Single crystals of 6H-SiC wafers were sequentially co-implanted with 360 keV Cs and I ions to a fluence of 1×10^{16} cm^{-2} at room temperature. The Monte Carlo simulation code, Stopping and Range of Ions in Matter (SRIM) was used to simulate the implanted ions in SiC. The SRIM simulation showed that in the co-implanted 6H-SiC, the initial implantation of Cs ions at a dose of 36 displacements per atom (dpa) highly amorphized the SiC structure producing a shallow amorphous SiC (a-SiC) layer of about 200 nm, and the subsequent implantation of I ions at a dose of 35 dpa caused more amorphization, especially to partially distorted/disordered parts of the a-SiC layer. This was confirmed by Raman spectroscopy and imaging analysis which also revealed that ion implantation induced the appearance of several new Si—Si and C—C homonuclear and Si—C heteronuclear bonds in the a-SiC network. The homonuclear bonds play a vital role in amorphization which proceeds through the accumulation of Frenkel pairs and antisite defects. The line-shapes of the Raman signals recorded for a-SiC layer resembles that of amorphous SiC, in the spectral region characteristic of homonuclear bonds in particular.

1. Introduction

Modern high-temperature nuclear reactors mostly use a triple-coated isotropic (TRISO) fuel particle-containing SiC layer which is designed to act as the main diffusion barrier layer for radioactive fission products, thus restricting these fission products from escaping the fuel particle under normal operation or accidents, making nuclear reactors inherently safe. In addition to the SiC layer of the TRISO fuel particle, the kernel is coated by other individual layers of pyrolytic carbon that have other functions, and all these layers are manufactured by chemical vapour deposition. The interest in SiC as a material for applications in nuclear power reactors arises from its ability to retain most of its properties at high temperatures [1]. Silicon carbide has low critical temperature for amorphization (e.g. for neutron irradiation T_c = 150 °C [2,3]), a great hardness (~9.3 Moh [1]), high corrosion resistance and relatively high thermal conductivity. Other than in TRISO fuel particle, SiC has many application possibilities due to its wide bandgap, for instance, it can be used in high-temperature ultraviolet sensors, radiation detectors and power electronics [4].

For TRISO fuel particle, some of the most important fission products which if leaked out would cause radiological danger are ^{88}Kr, ^{90}Sr, ^{110m}Ag, ^{131}Cs and ^{137}Cs, ^{134}I and ^{133}Xe [1,5], however, these are retained quite effectively by SiC layer up to temperatures of 1000 °C. There is a large number of systematic studies on the diffusion of these fission products in ion-implanted/irradiated 3C-SiC, 4H-SiC and 6H-SiC at temperatures above 1000 °C, including the evaluation of the structural response of the silicon carbides to the radiation damage and annealing [1]. Most of these studies used ion beam analysis techniques, i.e. Rutherford backscattering spectrometry (RBS) ion-channeling [6–17] and elastic recoil detection analysis (ERDA) [15,18], including transmission/scanning electron microscopy [16,17,19–26]. The optical vibration spectroscopies due to their ability to distinguish features of the crystalline-to-amorphous (c-a) transition in silicon carbides have also received attention [27–32], especially, Raman spectroscopy which provides details on the chemical reordering/disordering of ion bombardment-induced damage in SiC [33–36].

Previous studies have reported the Raman spectroscopy analyses of the ion bombardment-induced amorphous layer in SiC and observed that ion bombardment leads to the disappearance of the Raman signal intensities of the first-order bands of SiC and the appearance of new bands [18,28,33–38]. Most of these studies show the Raman signals which display only the Si–Si band at ~500 cm^{-1} in the spectral region characteristic of Si–Si bonds (~170–600 cm^{-1}), particularly, for ion bombardment-induced amorphous layer in SiC (see Ref. [8,9,16,18,28,33,37–39]). However, Sorieul et al. reported an extra Si—Si band at 200 cm^{-1} for the ion bombardment-induced amorphous layer in 6H-SiC at room temperature [36]. Nonetheless, the Raman signals recorded in these studies for

* Corresponding author.
E-mail address: mmadito@tlabs.ac.za (M.J. Madito).

https://doi.org/10.1016/j.apsusc.2020.148099
Received 30 July 2020; Received in revised form 11 September 2020; Accepted 5 October 2020
Available online 08 October 2020
0169-4332/

amorphous SiC (a-SiC) layer have different line-shapes compared to the typical Raman spectrum of amorphous SiC [40], in the spectral region characteristic of Si—Si bonds in particular. On the contrary, our study reports the Raman signal of the a-SiC layer (induced in 6H-SiC by Cs and I ions co-implantation at room temperature) which resembles that of amorphous SiC [40], and displays three broad Si–Si bands at 186, 266 and 480 cm^{-1} (characteristic frequencies of amorphous Si). This includes several new broad bands observed in the frequency regions of Si—C and C—C bonds.

2. Experimental

Single crystals of 6H-SiC wafers from *Intrinsic Semiconductors*® were sequentially co-implanted with 360 keV Cs and I ions to a fluence of 1×10^{16} cm^{-2} at room temperature. During implantation, the beam was raster scanned to achieve uniformity. To minimize the channelling effects, the normal to the crystal surface was tilted by 7° with respect to the primary ion beam. SRIM-2013 (Detailed Calculation with full Damage Cascades) was used to simulate the implanted Cs and I ions in silicon carbide. SRIM was carried out using C and Si threshold displacement energies of 20 and 35 eV respectively [41], the lattice binding energies of zero [42], and SiC density of 3.21×10^3 kg m^{-3}. The WITec alpha300 confocal Raman microscope and Project FIVE software were used for analyses. The 532 nm excitation laser set to 5 mW before the objective, and the 100× air objective with a numerical aperture of 0.9 which gives a diffraction-limited lateral resolution of ~360 nm (the spectral resolution is ~1 cm^{-1}) were used. The spectra were measured in the wide frequency range (0–3750 cm^{-1}). The confocal depth resolution was obtained as 0.7 μm by scanning the surface of the virgin 6H-SiC sample towards the focus of the laser beam. In a confocal Raman microscope, the focused illumination and spatially filtered detection allow only light from the focal plane to reach the detector, hence allowing optical sectioning (depth profiling) in transparent samples. Therefore, the cross-sectional depth profile imaging of the ion-implanted samples was obtained. The *z*-scan depth profile images were acquired over a width and depth of 6 μm (normalized to the thickness of the ion-implanted layer) with 100 points per line and 100 lines per image, and an integration time of 2 s. The average single Raman spectra were acquired over 15 s and 10 accumulations. No background subtraction or smoothing was applied to the Raman data.

3. Results and discussion

Fig. 1 displays SRIM results of 360 keV Cs and I ions implanted into SiC. As illustrated in Fig. 1(a), the I ions were implanted into Cs implanted SiC, although, the SRIM simulation was carried out for I ions implanted in SiC. Fig. 1(b) and (c) display the trajectories of 360 keV Cs and I ions in SiC, respectively. The subcascades generated by recoils in SiC are displayed in Fig. 1(d) and (e) for Cs and I ions, respectively. Cs and I ions distributions in SiC display the projected mean range, R_p of 105.5 and 99.9 nm, respectively. The observed discrepancy in the R_p values of Cs and I ions is as a result of their different ion masses since an approximate measure of the projected range is given by [43]

$$R_p \cong \frac{R}{1 + (M_2/3M_1)} \tag{1}$$

where the range, R, is the total distance that the projectile travels in coming to rest. M_1 and M_2 are the masses of the incident ion and the target atom, respectively.

To assess damage produced by ions in SiC the SRIM vacancies produced by Cs and I ions were converted into displacements per atom (dpa), as shown in Fig. 1(f), using the following expression [43]:

$$dpa = \frac{(Vacancies/ion \cdot Å) \times 10^8}{N_a} \times \varphi \tag{2}$$

where φ (ions/cm^2) is the ion fluence, N_a is the atomic density ($N_a = 9.64 \times 10^{22}$ atoms/cm^3).

In the ion-implanted SiC layer, the maximum nuclear energy loss values are 1.652 and 1.597 keV/nm which correspond to approximately 36 and 35 dpa of Cs and I ions, respectively. These dpa values are higher than the threshold value (0.28 dpa) required for the amorphization of SiC [36]. Also, the total dpa (i.e. the sum of dpa values of Cs and I ions) for a co-implanted sample is much higher. Therefore, in the co-implanted sample, the initial implantation of Cs ions highly amorphized the SiC structure producing a shallow a-SiC layer, and the subsequent implantation of I ions caused more amorphization in the a-SiC layer. During ion implantation, as the number of incident ions increases the ion trajectories overlap causing the overlap of damage cascades which yield coalescence of small clusters forming amorphous domains. The further coalescence of the clusters with amorphous domains forms large amorphous regions/layer. Molecular dynamics simulations have shown that these amorphous domains consist of Frenkel pairs and antisite defects which suggest that the driving force for c-a transition in SiC is the accumulation of Frenkel pairs and antisite defects [44]. In Fig. 1(f), the dpa values decrease to the amorphization threshold value (0.28 dpa) at the depth of about 200 nm suggesting that the amorphous layer is ~200 nm thick.

Moreover, the Raman spectroscopy and imaging depth profiles were used to probe chemical disorder in the a-SiC layer. As seen from SRIM simulation results the a-SiC layer has a thickness of approximately 200 nm, therefore, for Raman to probe such a thin layer the excitation laser wavelength with much shorter optical penetration depth is required. The Raman signal for many absorbing materials originates from a sample volume defined by the excitation laser wavelength and the beam diameter. The scattered light intensity, I_s, integrated over a depth d, is [45,46]

$$I_s = I_0 D \int_0^d e^{-2\alpha x} dx = \frac{I_0 D}{2\alpha}(1 - e^{-2\alpha d}) \tag{3}$$

and from the depth d to infinity is expressed as

$$I_d = I_0 D \int_d^\infty e^{-2\alpha x} dx = \frac{I_0 D}{2\alpha} e^{-2\alpha d} \tag{4}$$

where I_0, D, and α are the incident light intensity, scattering cross-section, and photoabsorption coefficient, respectively. Assuming that the penetration depth, d_p, arises from the depth that satisfies the relationship $I_d/(I_s + I_d) = 0.1$, d_p is expressed as [45,46]

$$d_p = \frac{-\ln 0.1}{2\alpha} = \frac{2.3}{2\alpha} \tag{5}$$

From equation (5), the penetration depth of single-crystal SiC ($d_p = 9.3 \times 10^5$ nm) and amorphous SiC ($d_p = 46$ nm) were estimated for a 532 nm laser using the absorption coefficient data of the single crystal and amorphous SiC for different laser wavelengths reported in Ref. [47]. The shorter optical penetration depth at 532 nm in amorphous SiC will allow Raman probing of the a-SiC layer induced in 6H-SiC by ion-implantation. Also, for improved accuracy, the signal contributions of the crystalline SiC bulk in the Raman spectra of the a-SiC layer will be subtracted using the "true component analysis demixing of spectra" (data processing tool of a WITec Project FIVE software).

The characteristic Raman spectrum of 6H-SiC is presented in Fig. 2. From this figure, the observed Raman-active modes with A_1 and E_2 symmetries are identifiable from the previous studies [36,48–50]. Fig. 2(a) and (b) display the first-order Raman bands (*strong modes) and the second-order bands of 6H-SiC, respectively. The high-quality SiC allows the observation of weaker peaks of the second-order Raman bands [36]. The three-strong modes are observed at 767, 789 and 967 cm^{-1} and are primarily longitudinal (LO) or transverse (TO) optical modes and the weak modes are largely axial or planar. The second-order Raman peaks are 151 and 263 cm^{-1} E_2 planar or transverse acoustic (TA) modes and 503 cm^{-1} A_1 axial or longitudinal acoustic (LA) mode. The 1090–1220 cm^{-1} weak modes are in the range of sp^3-bonded carbon, and that at ~1380 cm^{-1} is attributed to sp^2-bonded carbon [40,51]. The peaks in the range 1524–1709 cm^{-1} are assigned to the optical branch of the second-order Raman spectrum. Typically,

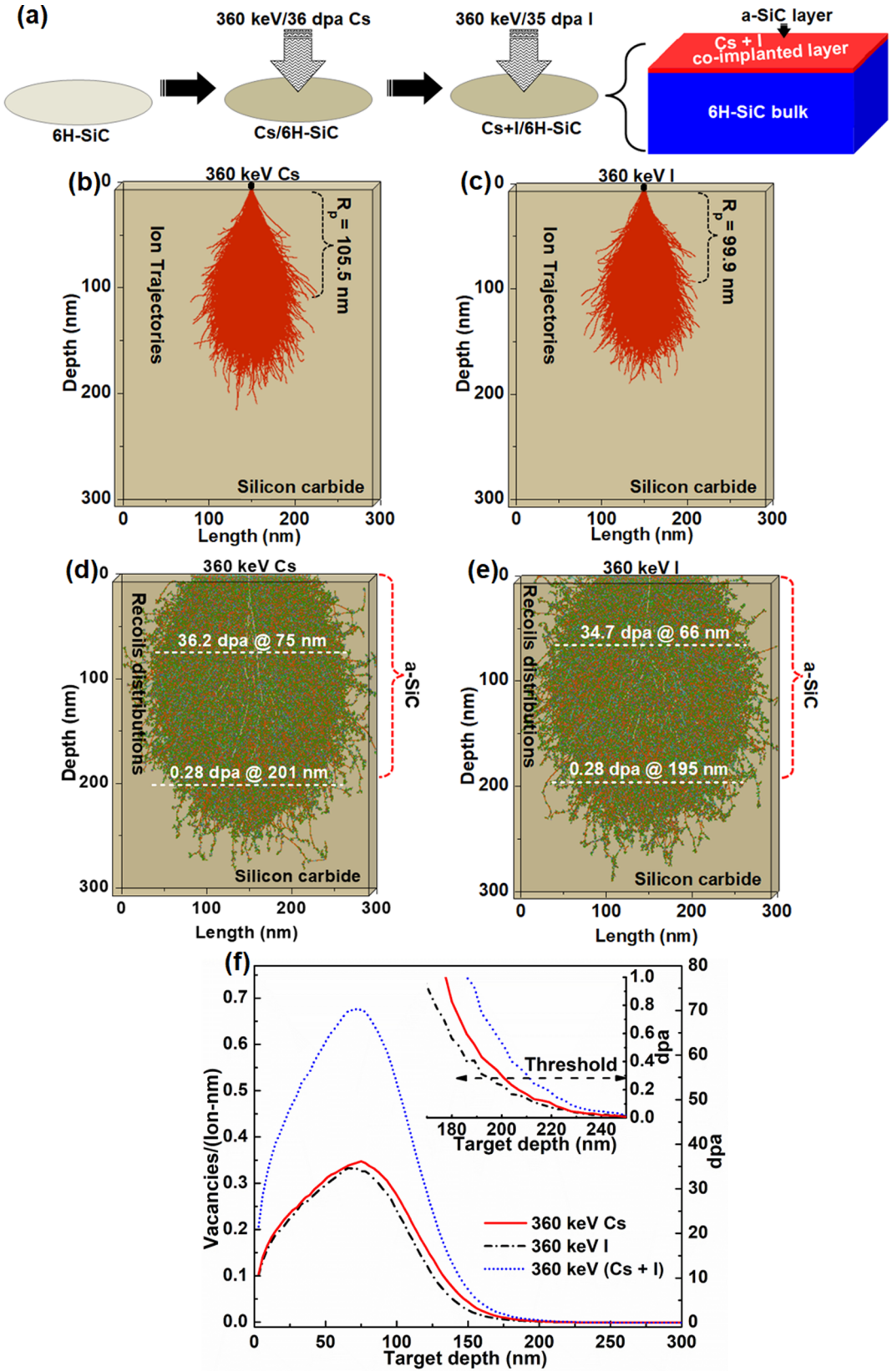

Fig. 1. (a) Schematic illustration of the Cs and I ions co-implanted 6H-SiC. SRIM calculations of co-implanted 360 keV Cs and I ions in 6H-SiC: (b) Cs and (c) I ions trajectories in SiC. (d) and (e) The subcascades generated by recoiling lattice atoms along the Cs and I ions trajectories, respectively, in SiC. (f) Target-atom vacancies distributions and the corresponding displacements per atom.

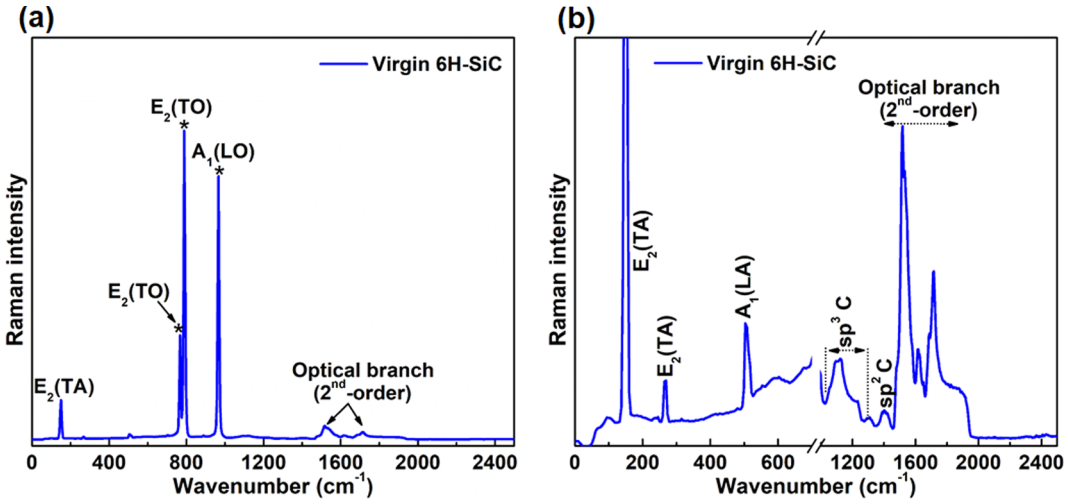

Fig. 2. Raman spectrum of the virgin 6H-SiC: The first-order peaks (*strong modes) and (b) the second-order peaks.

the second-order Raman spectrum reflects the whole Brillouin zone, and the one-phonon Raman spectrum reflects phonons at the Γ point of the Brillouin zone [52,53].

To distinguish the SiC structure of the shallow layer and the bulk of the ion-implanted 6H-SiC, the true component data processing of the acquired spectral data set of the Raman imaging depth profiles of the samples was carried out to obtain the intensity distribution images (Fig. 4(a) and (b)) and the corresponding average component spectra (Fig. 4(c)). As part of the true component data analysis, the demixing of spectra was carried out to subtract the contributions of the crystalline SiC bulk from the average Raman spectrum of the a-SiC layer, as shown in Fig. 3(a)

and the standard spectrum used was obtained from the virgin 6H-SiC sample. Consequently, approximately 1.5% of the intensity of the first-order bands of the crystalline SiC bulk was subtracted from the average signal of the a-SiC layer. In Fig. 3(b), the Raman spectrum from the surface (*z*-scan depth of 0 μm) of the a-SiC layer does not show the signal contributions of the SiC bulk and is similar to the average Raman spectrum of the amorphous layer after demixing which suggests that the Raman spectra of the a-SiC layer with the bulk contributions were acquired at deeper *z*-scan depth (> 0.1 μm), as expected. In Fig. 4(a–c), the true component analysis (plus demixing of spectra) displays two distinct parts of the ion-implanted samples, i.e. ~200 nm thick a-SiC layer and the crystalline 6H-SiC bulk which show typical Raman spectra of the amorphous SiC (red graphs) [40] and crystalline 6H-SiC (blue graph), respectively.

Moreover, in Fig. 4(c), the two Raman spectra of the a-SiC layer are similar which confirm that the initial implantation of Cs ions highly amorphized the crystal structure of the a-SiC layer and the subsequent implantation of I ions caused more structural amorphization as suggested by higher intensity Raman signal of the co-implanted sample. In contrast to the Raman spectrum of the crystalline 6H-SiC bulk, the Raman spectra of the a-SiC layer display additional features associated with amorphous Si—Si (~170–600 cm^{-1}), Si—C (~650–1000 cm^{-1}), and C—C (~1100–1650 cm^{-1}) bonds. Previous studies have proposed that the structure of a-SiC is made of C—C bonds (mixed sp^2/sp^3) mainly dispersed in the tetrahedral networks of Si—C and Si—Si [54–57]. It is worth noting that the C—C bonds of the a-SiC layer display high-intensity peaks relative to the heteropolar bonds but despite the high intensity, the relative amount of these homonuclear bonds is about a few percent [54]. The high-intensity signal of the C—C bonds could be due to the high bonds' polarizability of C—C which is greater than the Si—C bond polarizability [54]. Gorman et al. have observed a similar relative intensity of the C—C homonuclear and Si—C heteropolar bonds in carbon deficient amorphous SiC sample [40]. Nonetheless, the homonuclear ratio can be calculated from the Raman signal, however, such calculation would require the laser excitation cross-sections of both homonuclear and heteronuclear bonds in the sample which are

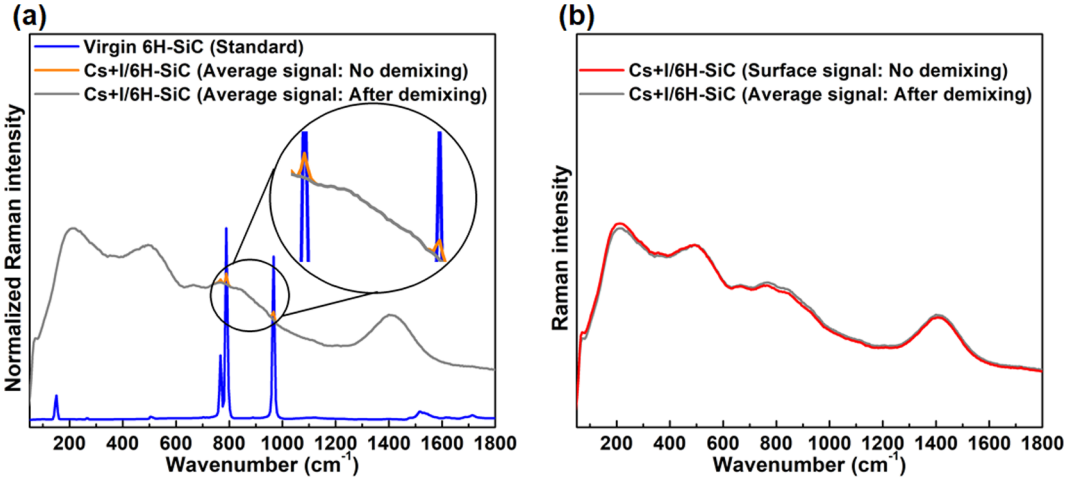

Fig. 3. The demixing of spectra (True component analysis): (a) The Raman spectrum of the virgin 6H-SiC and the average Raman spectrum of the a-SiC layer with and without demixing of spectra. (b) The Raman spectrum from the surface of the a-SiC layer and the average Raman spectrum of the amorphous layer after demixing in (a).

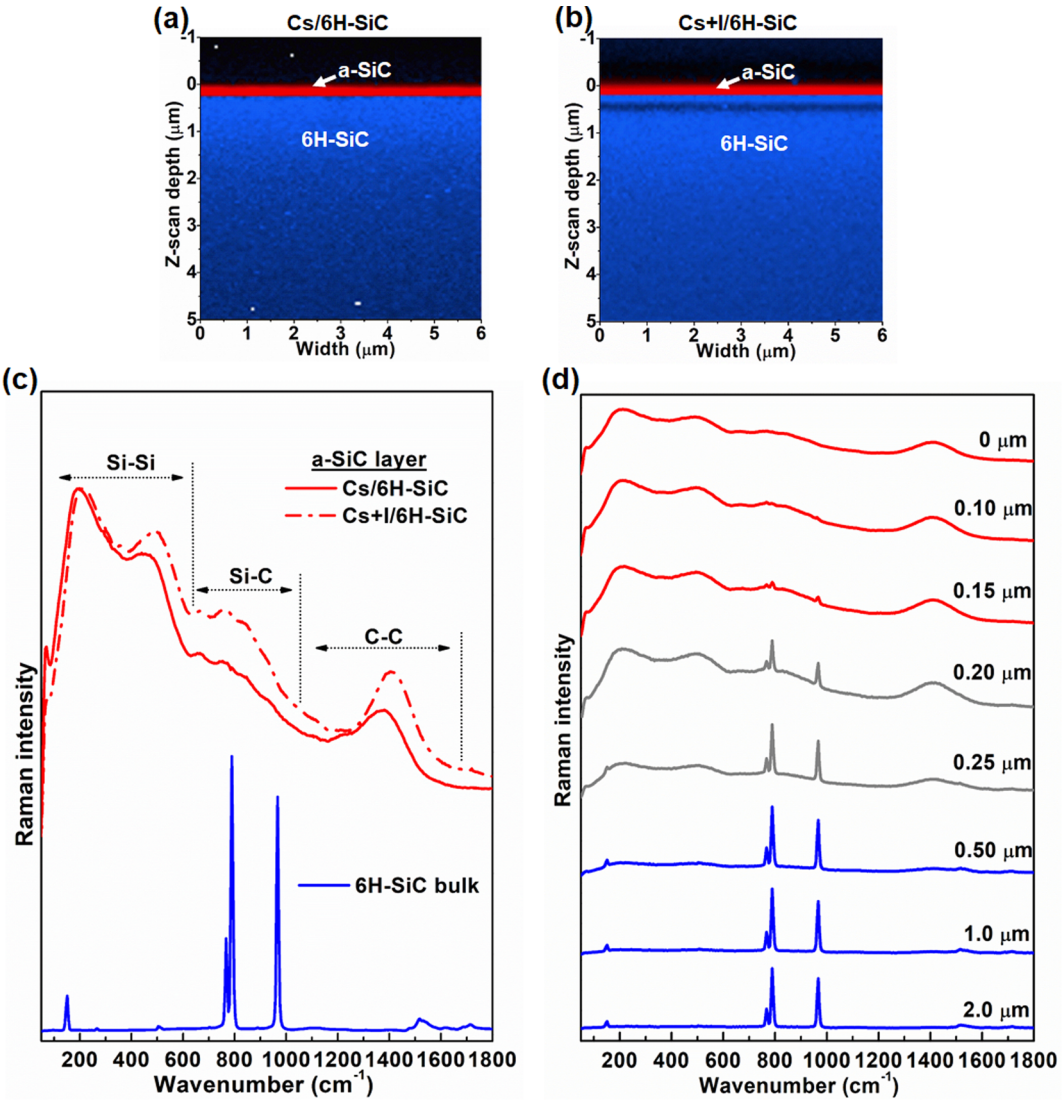

Fig. 4. True component mapping (Raman imaging depth profiles) of (a) Cs ion-implanted and (b) Cs and I ions co-implanted 6H-SiC, and (c) the corresponding components average spectra. (d) confocal Raman spectra of the co-implanted sample at various z-scan depths.

unknown or either a reference sample with a well-known content of these two different bonds. Fig. 4(d) shows the confocal Raman spectra of the co-implanted sample at various *z*-scan depths. From this figure, the Raman spectra for the shallow *z*-scan depth of 0, 0.10 and 0.15 μm (red graphs) show typical Raman spectra of the amorphous SiC and that for the deeper *z*-scan depth of 0.5, 1.0 and 2.0 μm (blue graphs) display typical spectra of crystalline 6H-SiC. The interface spectra at the *z*-scan depth of 0.2 and 0.25 μm (grey graphs) show mixed features of amorphous/distorted and crystalline silicon carbide.

The three frequency regions of the Raman spectra of a-SiC were deconvoluted using the combination of Gaussian and Lorentzian functions and the positions of the peaks compared with previous studies [36,48,49,53,58,59], as shown in Fig. 5. Typically, the second-order Raman spectrum of crystalline 6H-SiC displays weak and narrow 263 cm^{-1} E_2(TA) and 503 cm^{-1} A_1(LA) optical modes (see Fig. 2), which in a-SiC layer shift to new frequencies (i.e. from 263 to 266 cm^{-1} and from 503 to 480 cm^{-1}) and have shape characteristic of the pronounced broad peaks (fitting peaks in Fig. 5(a)) of amorphous Si [60,61]. In this case, the Raman selection rules and wavevector conservation are no longer valid due to the crystal amorphization, therefore, all phonons are optically allowed and the Raman spectrum resembles the phonon density of states [59,62]. The broadband at 186 cm^{-1} is also related to Si–Si vibrations of amorphous Si [36]. Additionally, the cumulative fit of these peaks is similar (R^2 = 0.998) to the line-shape of the Raman signal of the a-SiC layer in the spectral region characteristic of Si—Si bonds which resemble that of amorphous SiC [40]. This confirms the presence of highly disordered Si—Si bonds in the a-SiC network. The accumulation of Frenkel pairs and antisite defects which drive c-a transition in SiC leads to local residual strain due to the difference in the atomic sizes of Si and C, and the chemical preference of homonuclear bonds formation, creating significant compressive stress in the SiC lattice [63,64]. It is well known that radiation-induced damage causes lattice swelling in SiC [65,66]. This could explain the observed bands' shifts of the a-SiC layer as compared to the virgin sample. Furthermore, in the frequency region of Si—C bonds, the strong and narrow 789 cm^{-1} E_2(TO) and 967 cm^{-1} A_1(LO) optical modes disappeared and the new low-intensity broad bands appeared at 670, 766, 849 and 923 cm^{-1} upon implantation (Fig. 5(b)), which are attributed to amorphous SiC. In the spectral region characteristic of C—C bonds, the ion-implanted 6H-SiC samples display the broadband at about 1400 cm^{-1} characteristic of amorphous sp^2 carbon which has a shoulder at ~1220 cm^{-1} associated with sp^3 hybridization [51]. This band is a mixture of sp^2/sp^3 coordination in the distorted Si-C network. It has been shown through molecular dynamics simulations that C—C homonuclear bonds play a vital role in SiC structural amorphization

before amorphization, the accumulated defects are mainly C Frenkel pairs (67%) with 18% Si Frenkel pairs and 15% antisite defects [67].

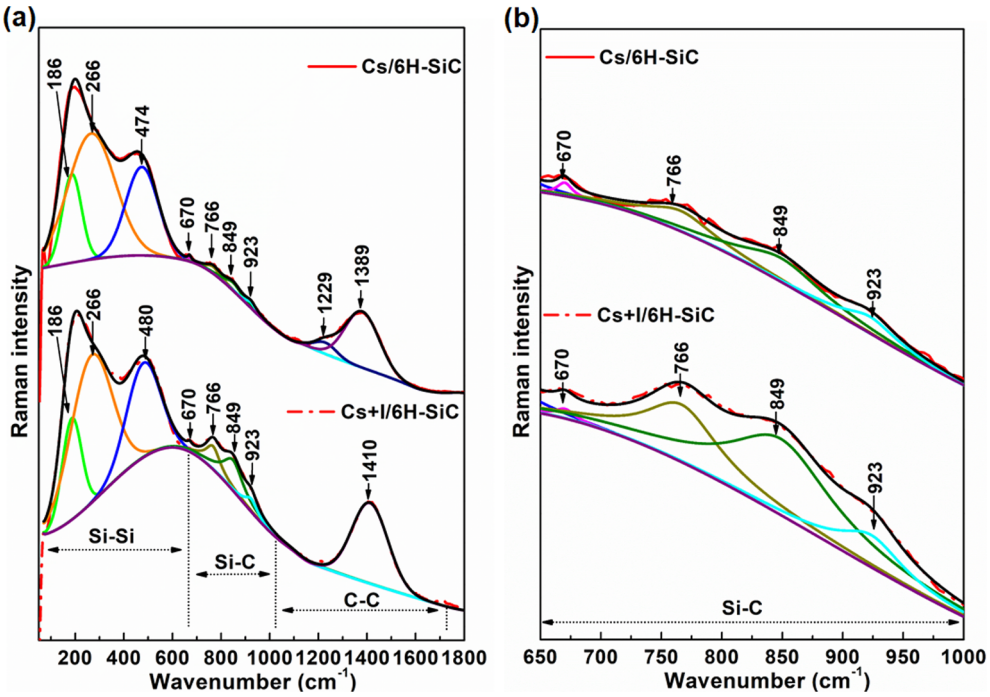

Fig. 5. (a) Deconvoluted average Raman spectra of the a-SiC layer in Fig. 3(c). (b) The deconvoluted frequency region of Si—C bonds in (a).

Also, this simulation study has demonstrated that SiC can be amorphized exclusively by C displacements at a dose of 0.2 dpa with a decrease in density of ~15% [67]. The assignment of the Raman peaks of the crystalline 6H-SiC and the ion-implanted samples are summarized in Tables 1 and 2.

4. Conclusion

A detailed investigation (SRIM and Raman analyses) of the chemical disorder of a-SiC layer induced in 6H-SiC by Cs and I ions co-implantation have been presented. It was found that in the co-implantation of the single crystals of 6H-SiC wafers at room temperature, the initial implantation of cesium at a dose of 36 dpa highly amorphized the SiC structure producing a 200 nm a-SiC layer, and the subsequent implantation of iodine at approximately the same dose caused more amorphization in the a-SiC layer, especially to partially distorted/disordered regions of the layer. Nevertheless, the Cs and I dose of about 36 dpa (at room temperature) used in this study is higher than the minimum value (0.28 dpa) required for amorphization of SiC at low temperatures [1,68]. It was also found that ion implantation induced not only amorphization of the SiC structure but also the appearance of several new Si—Si and C—C homonuclear and Si—C heteronuclear bonds in the a-SiC network in agreement with similar previous studies. The homonuclear bonds play a vital role in SiC amorphization. It has been shown that before amorphization, the accumulated defects are 67% C Frenkel pairs 18% Si Frenkel pairs and 15% antisite defects

and C displacements at 0.2 dpa highly amorphized SiC [67]. Consequently, SiC amorphization proceeds through the accumulation of Frenkel pairs and antisite defects. Furthermore, the line-shapes of the Raman signals recorded for the a-SiC layer resembles that of amorphous SiC [40], especially in the spectral region characteristic of Si—Si bonds. On the contrary, most of the previous studies which reported the Raman signals recorded for ion bombardment-induced amorphous layer in crystalline SiC at room temperature show different line-shapes in the frequency region of Si—C bonds compared to that of amorphous SiC [40]. It is worth noting that a 532 nm laser has a shorter optical penetration depth of about 46 nm in amorphous SiC which made it possible to probe a thin shallow layer of a-SiC, and for improved accuracy, the minor contributions of the crystalline SiC bulk in the signals of the a-SiC layer (acquired at deeper *z*-scan depth) were subtracted using the

Table 1
The bands from Fig. 2 and the deconvoluted average Raman spectra in Fig. 5. The values in the parentheses are the bands' FWHMs. The shaded cells show the new bands and the bands with dramatic broadening upon ion implantation in the a-SiC layer.

	Si–C vibrations bands (cm^{-1})							
	E_2(TA)		E_2(TO)	E_2(TO)			A_1(LO)	Optical branch
Virgin 6H-SiC	151* (9.2)	–	767* (9.6)	789* (9.6)	–	–	967* (9.3)	1524-1709
Cs/6H-SiC	–	670 (15.6)	766 (66.0)	–	849 (80.0)	923 (50.3)	–	–
Cs + I/6H-SiC	–	670 (20.0)	766 (74.4)	–	849 (101.1)	923 (62.0)	–	–

*Strong modes.

Table 2
The bands from Fig. 2 and the deconvoluted average Raman spectra in Fig. 5. The values in the parentheses are the bands' FWHMs. The shaded cells show the new bands and the bands with dramatic broadening upon ion implantation in the a-SiC layer.

	Si–Si vibrations bands (cm^{-1})			C–C vibrations bands (cm^{-1})		
	E_2(TA)	E_2(TA)	A_1(LA)			
Virgin 6H-SiC	–	263♦ (7.70)	503♦ (14.9)	1090-1130♦ (91.5)	1220♦ (22.3)	1380♦ (56.1)
Cs/6H-SiC	186 (92.8)	266 (228.2)	474 (156.5)	–	1229 (107.6)	1389 (165.5)
Cs + I/6H-SiC	186 (94.0)	266 (200.2)	480 (162.4)	–	–	1410 (174.0)

♦Weak modes.

data processing tool of a WITec Project FIVE software. Nevertheless, similar Raman signals of the a-SiC layer can be obtained using UV laser which has a much shorter optical penetration depth of ~10 nm in a-SiC.

CRediT authorship contribution statement

M.J. Madito: Conceptualization, Methodology, Investigation, Validation, Writing - original draft. **T.T. Hlatshwayo:** Supervision, Funding acquisition, Resources. **C.B. Mtshali:** Supervision, Resources.

Declaration of Competing Interest

The authors declare that they have no known competing financial interests or personal relationships that could have appeared to influence the work reported in this paper.

Acknowledgements

This work is based on the research supported by the National Research Foundation of South Africa (NRF) via iThemba LABS Materials Research Department (MRD) and the University of Pretoria (South Africa). Prof. E. Wendler and her team, Institut für Festkörperphysik, Friedrich-Schiller University, Jena, Germany are acknowledged for ion implantation.

References

[1] J.B. Malherbe, Diffusion of fission products and radiation damage in SiC, J. Phys. D. Appl. Phys. 46 (2013) 473001.
[2] L.L. Snead, T. Nozawa, Y. Katoh, T.S. Byun, S. Kondo, D.A. Petti, Handbook of SiC properties for fuel performance modeling, J. Nucl. Mater. 371 (2007) 329–377, https://doi.org/10.1016/j.jnucmat.2007.05.016.
[3] G. Newsome, L.L. Snead, T. Hinoki, Y. Katoh, D. Peters, Evaluation of neutron irradiated silicon carbide and silicon carbide composites, J. Nucl. Mater. 371 (2007) 76–89, https://doi.org/10.1016/j.jnucmat.2007.05.007.
[4] A.M. Ivanov, N.B. Strokan, D.V. Davydov, N.S. Savkina, A.A. Lebedev, Y.T. Mironov, G.A. Riabov, E.M. Ivanov, Radiation hardness of SiC based ions detectors for influence of the relative protons, Appl. Surf. Sci. 184 (2001) 431–436, https://doi.org/10.1016/S0169-4332(01)00529-3.
[5] K. Minato, T. Ogawa, K. Fukuda, H. Sekino, H. Miyanishi, S. Kado, I. Takahashi, Release behavior of metallic fission products from HTGR fuel particles at 1600 to 1900°C, J. Nucl. Mater. 202 (1993) 47–53, https://doi.org/10.1016/0022-3115(93)90027-V.
[6] E. Wendler, A. Heft, W. Wesch, Ion-beam induced damage and annealing behaviour in SiC, Nucl. Instrum. Meth. Phys. Res. Sect. B Beam Interact. Mater. Atoms. 141 (1998) 105–117, https://doi.org/10.1016/S0168-583X(98)00083-4.
[7] Y. Katoh, N. Hashimoto, S. Kondo, L.L. Snead, A. Kohyama, Microstructural development in cubic silicon carbide during irradiation at elevated temperatures, J. Nucl. Mater. 351 (2006) 228–240, https://doi.org/10.1016/j.jnucmat.2006.02.007.
[8] E. Viswanathan, Y.S. Katharria, S. Selvakumar, A. Arulchakkaravarthi, D. Kanjilal, K. Sivaji, Investigations on the structural and optical properties of the swift heavy ion irradiated 6HSiC, Nucl. Instrum. Meth. Phys. Res. Sect. B Beam Interact. Mater. Atoms. 269 (2011) 1103–1107, https://doi.org/10.1016/j.nimb.2011.01.017.
[9] E. Wendler, T. Bierschenk, F. Felgenträger, J. Sommerfeld, W. Wesch, D. Alber, G. Bukalis, L.C. Prinsloo, N. Van Der Berg, E. Friedland, J.B. Malherbe, Damage formation and optical absorption in neutron irradiated SiC, in: Nucl. Instruments Methods Phys. Res. Sect. B Beam Interact. with Mater. Atoms, North-Holland, 2012: pp. 97–101. doi:10.1016/j.nimb.2012.01.010.
[10] L.L. Snead, S.J. Zinkle, J.C. Hay, M.C. Osborne, Amorphization of SiC under ion and neutron irradiation, Nucl. Instrum. Meth. Phys. Res. Sect. B Beam Interact. Mater. Atoms. 141 (1998) 123–132, https://doi.org/10.1016/S0168-583X(98)00085-8.
[11] A. Benyagoub, A. Audren, L. Thomé, F. Garrido, Athermal crystallization induced by electronic excitations in ion-irradiated silicon carbide, Appl. Phys. Lett. 89 (2006) 241914, , https://doi.org/10.1063/1.2405410.
[12] W.J. Weber, W. Jiang, S. Thevuthasan, Defect annealing kinetics in irradiated 6H-SiC, Nucl. Instrum. Meth. Phys. Res. Sect. B Beam Interact. Mater. Atoms. 166 (2000) 410–414, https://doi.org/10.1016/S0168-583X(99)00868-X.
[13] Y. Zhang, W.J. Weber, W. Jiang, A. Hallén, G. Possnert, Damage evolution and recovery on both Si and C sublattices in Al-implanted 4H-SiC studied by Rutherford backscattering spectroscopy and nuclear reaction analysis ARTICLES YOU MAY BE INTERESTED IN, J. Appl. Phys. 91 (2002) 6388, https://doi.org/10.1063/1.1469204.
[14] X. Kerbiriou, J.M. Costantini, M. Sauzay, S. Sorieul, L. Thoṁ, J. Jagielski, J.J. Grob, Amorphization and dynamic annealing of hexagonal SiC upon heavy-ion irradiation: effects on swelling and mechanical properties, J. Appl. Phys. 105 (2009) 073513, , https://doi.org/10.1063/1.3103771.
[15] W. Jiang, W.J. Weber, C.M. Wang, Y. Zhang, Disordering behavior and helium diffusion in He+ irradiated 6H-SiC, J. Mater. Res. 17 (2002) 271–274, https://doi.org/10.1557/JMR.2002.0038.
[16] T.T. Hlatshwayo, J.B. Malherbe, N.G. Van Der Berg, L.C. Prinsloo, A.J. Botha, E. Wendler, W. Wesch, Annealing of silver implanted 6H-SiC and the diffusion of the silver, Nucl. Instrum. Meth. Phys. Res. Sect. B Beam Interact. Mater. Atoms. 274 (2012) 120–125, https://doi.org/10.1016/j.nimb.2011.12.006.
[17] T.T. Hlatshwayo, J.B. Malherbe, N.G. Van Der Berg, A.J. Botha, P. Chakraborty, Effect of thermal annealing and neutron irradiation in 6H-SiC implanted with silver at 350 °c and 600 °c, in: Nucl. Instruments Methods Phys. Res. Sect. B Beam Interact. with Mater. Atoms, North-Holland, 2012: pp. 61–64. doi:10.1016/j.nimb.2011.07.039.
[18] W. Jiang, Y. Zhang, M.H. Engelhard, W.J. Weber, G.J. Exarhos, J. Lian, R.C. Ewing, Behavior of Si and C atoms in ion amorphized SiC, J. Appl. Phys. 101 (2007) 023524, , https://doi.org/10.1063/1.2431941.
[19] T. Iseki, T. Maruyama, T. Yano, T. Suzuki, T. Mori, Effects of neutron irradiation and subsequent annealing on strength and toughness of SiC ceramics, J. Nucl. Mater. 170 (1990) 95–100, https://doi.org/10.1016/0022-3115(90)90330-P.
[20] D.J. Senor, G.E. Youngblood, L.R. Greenwood, D.V. Archer, D.L. Alexander, M.C. Chen, G.A. Newsome, Defect structure and evolution in silicon carbide irradiated to 1 dpa-SiC at 1100 °C, J. Nucl. Mater. 317 (2003) 145–159, https://doi.org/10.1016/S0022-3115(03)00077-1.
[21] T. Yano, H. Miyazaki, M. Akiyoshi, T. Iseki, X-ray diffractometry and high-resolution electron microscopy of neutron-irradiated SiC to a fluence of 1.9 × 1027 n/m2, J. Nucl. Mater. 253 (1998) 78–86. doi:10.1016/S0022-3115(97)00331-0.
[22] R.J. Price, Neutron irradiation-induced voids in β-silicon carbide, J. Nucl. Mater. 48 (1973) 47–57, https://doi.org/10.1016/0022-3115(73)90077-9.
[23] J. Cabrero, F. Audubert, R. Pailler, A. Kusiak, J.L. Battaglia, P. Weisbecker, Thermal conductivity of SiC after heavy ions irradiation, J. Nucl. Mater. 396 (2010) 202–207, https://doi.org/10.1016/j.jnucmat.2009.11.006.
[24] K. Hojou, S. Furuno, H. Otsu, K. Izui, T. Tsukamoto, In-situ observation system of the dynamic process of structual changes during ion irradiation and its application to SiC and TiC crystals, J. Nucl. Mater. 155–157 (1988) 298–302, https://doi.org/10.1016/0022-3115(88)90258-9.
[25] J.B. Malherbe, N.G. Van Der Berg, A.J. Botha, E. Friedland, T.T. Hlatshwayo, R.J. Kuhudzai, E. Wendler, W. Wesch, P. Chakraborty, E.F. Da Silveira, SEM analysis of ion implanted SiC, Nucl. Instrum. Meth. Phys. Res. Sect. B Beam Interact.

Mater. Atoms. 315 (2013) 136–141, https://doi.org/10.1016/j.nimb.2013.04.073.
[26] E. Friedland, J.B. Malherbe, N.G. van der Berg, T. Hlatshwayo, A.J. Botha, E. Wendler, W. Wesch, Study of silver diffusion in silicon carbide, J. Nucl. Mater. 389 (2009) 326–331, https://doi.org/10.1016/j.jnucmat.2009.02.022.
[27] D.J. Brink, J.B. Malherbe, J. Camassel, Neutron irradiation effects in SiC, Nucl. Instrum. Meth. Phys. Res. Sect. B Beam Interact. Mater. Atoms. 267 (2009) 2716–2718, https://doi.org/10.1016/j.nimb.2009.05.029.
[28] Z.C. Feng, S.C. Lien, J.H. Zhao, X.W. Sun, W. Lu, Structural and optical studies on ion-implanted 6H-SiC thin films, Thin Solid Films 516 (2008) 5217–5222, https://doi.org/10.1016/j.tsf.2007.07.094.
[29] S. Nakashima, T. Mitani, J. Senzaki, H. Okumura, T. Yamamoto, Deep ultraviolet Raman scattering characterization of ion-implanted SiC crystals, J. Appl. Phys. 97 (2005) 123507, , https://doi.org/10.1063/1.1931039.
[30] L. Li, S. Prucnal, S.D. Yao, K. Potzger, W. Anwand, A. Wagner, S. Zhou, Rise and fall of defect induced ferromagnetism in SiC single crystals, Appl. Phys. Lett. 98 (2011) 222508, , https://doi.org/10.1063/1.3597629.
[31] T. Tsvetkova, P. Sellin, R. Carius, O. Angelov, D. Dimova-Malinovska, J. Zuk, Optical contrast formation in amorphous silicon carbide with high-energy focused ion beams, Nucl. Instrum. Meth. Phys. Res. Sect. B Beam Interact. Mater. Atoms. 267 (2009) 1583–1587, https://doi.org/10.1016/j.nimb.2009.01.148.
[32] R.J. Kuhudzai, J.B. Malherbe, N.G. Van Der Berg, T.T. Hlatshwayo, O. Odutemowo, L.C. Prinsloo, A.V. Buys, R. Erasmus, E. Wendler, Deep ultra violet and visible Raman spectroscopy studies of ion implanted 6H-SiC: recrytallisation behaviour and thermal decomposition/thermal etching of the near surface region, Nucl. Instrum. Meth. Phys. Res. B 365 (2015) 342–346.
[33] W. Bolse, J. Conrad, T. Rödle, T. Weber, Ion-beam-induced amorphization of 6H-SiC, Surf. Coatings Technol. 74–75 (1995) 927–931, https://doi.org/10.1016/0257-8972(95)08288-3.
[34] W. Bolse, Formation and development of disordered networks in Si-based ceramics under ion bombardment, Nucl. Instrum. Meth. Phys. Res. Sect. B Beam Interact. Mater. Atoms. 141 (1998) 133–139, https://doi.org/10.1016/S0168-583X(98)00086-X.
[35] C.W. White, C.J. McHargue, P.S. Sklad, L.A. Boatner, G.C. Farlow, Ion implantation and annealing of crystalline oxides, Mater. Sci. Rep. 4 (1989) 41–146, https://doi.org/10.1016/S0920-2307(89)80005-2.
[36] S. Sorieul, J.M. Costantini, L. Gosmain, L. Thomé, J.J. Grob, Raman spectroscopy study of heavy-ion-irradiated α-SiC, J. Phys. Condens. Matter. 18 (2006) 5235–5251, https://doi.org/10.1088/0953-8984/18/22/022.
[37] W. Bolse, Formation and development of disordered networks in Si-based ceramics under ion ombardment, Nucl. Instrum. Meth. Phys. Res. Sect. B Beam Interact. Mater. Atoms. 141 (1998) 133–139, https://doi.org/10.1016/S0168-583X(98)00086-X.
[38] P. Musumeci, F. Roccaforte, R. Reitano, Angular distortion of Si clusters in a-SiC, Europhys. Lett. 55 (2001) 674–678.
[39] T.T. Hlatshwayo, J.H. O'Connell, V.A. Skuratov, M. Msimanga, R.J. Kuhudzai, E.G. Njoroge, J.B. Malherbe, Effect of Xe ion (167 MeV) irradiation on poly-crystalline SiC implanted with Kr and Xe at room temperature, J. Phys. D. Appl. Phys. 48 (2015) 465306, , https://doi.org/10.1088/0022-3727/48/46/465306.
[40] M. Gorman, S.A. Solin, Direct evidence for homonuclear bonds in amorphous SiC, Solid State Commun. 15 (1974) 761–765.
[41] R. Devanathan, W. Weber, Displacement energy surface in 3C and 6H SiC, J. Nucl. Mater. 278 (2000) 258–265, https://doi.org/10.1016/S0022-3115(99)00266-4.
[42] R.E. Stoller, M.B. Toloczko, G.S. Was, A.G. Certain, S. Dwaraknath, F.A. Garner, On the use of SRIM for computing radiation damage exposure, Nucl. Instrum. Meth. Phys. Res. Sect. B Beam Interact. Mater. Atoms. 310 (2013) 75–80, https://doi.org/10.1016/J.NIMB.2013.05.008.
[43] M. Nastasi, J.W. Mayer, J.K. Hirvonen (Eds.), Ion-solid Interactions: Fundamentals and Applications, Cambridge University Press, Cambridge, 1996.
[44] F. Gao, W.J. Weber, R. Devanathan, Defect production, multiple ion – solid interactions and amorphization in SiC, Nucl. Instrum. Meth. Phys. Res. B 191 (2002) 487–496.
[45] J.I. Takahashi, T. Makino, Raman scattering measurement of silicon-on-insulator substrates formed by high-dose oxygen-ion implantation, J. Appl. Phys. 63 (1988) 87–91, https://doi.org/10.1063/1.340467.
[46] I. De Wolf, Micro-Raman spectroscopy to study local mechanical stress in silicon integrated circuits, Semicond. Sci. Technol. 11 (1996) 139, https://doi.org/10.1088/0268-1242/11/2/001.
[47] G. Derst, C. Wilbertz, K.L. Bhatia, W. Krätschmer, S. Kalbitzer, Optical properties of SiC for crystalline/amorphous pattern fabrication, Appl. Phys. Lett. 54 (1989) 1722, https://doi.org/10.1063/1.101271.
[48] J.C. Burton, L. Sun, M. Pophristic, S.J. Lukacs, F.H. Long, Z.C. Feng, I.T. Ferguson, Spatial characterization of doped SiC wafers by Raman spectroscopy, J. Appl. Phys. 84 (1998) 6268, https://doi.org/10.1063/1.368947.
[49] S. Nakashima, H. Harima, Raman Investigation of SiC Polytypes, Phys. Status Solidi. 162 (1997) 39–64, https://doi.org/10.1002/1521-396X(199707)162:1<39::AID-PSSA39>3.0.CO;2-L.
[50] S. Sorieul, X. Kerbiriou, J.-M. Costantini, L. Gosmain, G. Calas, C. Trautmann, Optical spectroscopy study of damage induced in 4H-SiC by swift heavy ion irradiation, J. Phys. Condens. Matter. 24 (2012) 125801, , https://doi.org/10.1002/lary.20355.
[51] R.E. Shroder, R.J. Nemanich, J.T. Glass, Analysis of the composite structures in diamond thin films by Raman spectroscopy, Phys. Rev. B. 41 (1990) 3738–3745, https://doi.org/10.1103/PhysRevB.41.3738.
[52] D.W. Feldman, J.H. Parker, W.J. Choyke, L. Patrick, Raman scattering in 6H SiC, Phys. Rev. 170 (1968) 698–704, https://doi.org/10.1103/PhysRev.170.698.
[53] J.C. Burton, L. Sun, F.H. Long, Z.C. Feng, I.T. Ferguson, First- and second-order Raman scattering from semi-insulating 4H-SiC, Phys. Rev. B - Condens. Matter Mater. Phys. 59 (1999) 7282–7284, https://doi.org/10.1103/PhysRevB.59.7282.
[54] C. Meunier, B. Cros, J. Durand, Chemical bonding analysis of a-SiC" H films by Raman spectroscopy, J. Non-Cryst. Solids 169 (1994) 37–46.
[55] F. Finocchi, G. Galli, M. Parrinello, C.M. Bertoni, Microscopic struture of amorphous covalent alloys probed by *ab initio* molecular dynamics: SiC, Phys. Rev. Lett. 68 (1992) 3044–3047, https://doi.org/10.1103/PhysRevLett.68.3044.
[56] M.A. Petrich, K.K. Gleason, J.A. Reimer, Structure and properties of amorphous hydrogenated silicon carbide, Phys. Rev. B. 36 (1987) 9722–9731, https://doi.org/10.1103/PhysRevB.36.9722.
[57] C. Meneghini, S. Pascarelli, F. Boscherini, S. Mobilio, F. Evangelisti, Structural study of a-Si1-xCx: H by exafs and X-ray scattering, J. Non Cryst. Solids 137–138 (1991) 75–78, https://doi.org/10.1016/S0022-3093(05)80060-2.
[58] J.C. Burton, F.H. Long, I.T. Ferguson, Resonance enhancement of electronic Raman scattering from nitrogen defect levels in silicon carbide Raman scattering from anisotropic LO-phonon-plasmon-coupled mode in n-type 4H-and 6H, Cit. J. Appl. Phys. 86 (1999) 6268, https://doi.org/10.1063/1.371011.
[59] M. Hofmann, A. Zywietz, K. Karch, F. Bechstedt, Lattice dynamics of SiC polytypes within the bond-charge model, Phys. Rev. B. 50 (1994) 401–411.
[60] A. Zwick, R. Caries, Multiple-order Raman scattering in crystalline and amorphous silicon, Phys. Rev. B. 48 (1993) 6024–6032.
[61] M. Ehbrecht, H. Ferkel, F. Huisken, L. Holz, Y.N. Polivanov, V.V. Smirnov, O.M. Stelmakh, R. Schmidt, Deposition and analysis of silicon clusters generated by laser-induced gas phase reaction, J. Appl. Phys. 78 (1995) 5302–5306, https://doi.org/10.1063/1.360737.
[62] H. Hobert, H. Dunken, R. Menzel, T. Bachmann, W. Wesch, Infrared and Raman spectroscopy of particle-beam induced damage of silicon carbide, J. Non Cryst. Solids. 220 (1997) 187–194, https://doi.org/10.1016/S0022-3093(97)00305-0.
[63] A. Size, B. Covalent, Atomic size effects in pressure-induced of a binary covalent lattice, Phys. Rev. 75 (1995) 2738–2741.
[64] J. Li, Transformation strain by chemical disordering in silicon carbide, J. Appl. Phys. 6466 (2013) 49–53, https://doi.org/10.1063/1.1690093.
[65] M. Idzat, H. Konishi, M. Imai, Neutron irradiation swelling of SiC and SiC f/SiC for advanced nuclear applications, Energy Procedia 71 (2015) 328–336, https://doi.org/10.1016/j.egypro.2014.11.886.
[66] A.J. Leide, R.I. Todd, D.E.J. Armstrong, Measurement of swelling-induced residual stress in ion implanted SiC, and its effect on micromechanical properties, Acta Mater. 196 (2020) 78–87, https://doi.org/10.1016/j.actamat.2020.06.030.
[67] R. Devanathan, F. Gao, W.J. Weber, R. Devanathan, F. Gao, W.J. Weber, Amorphization of silicon carbide by carbon displacement, Appl. Phys. Lett. 3909 (2004) 1–4, https://doi.org/10.1063/1.1739515.
[68] Y. Pacaud, J. Stoemenos, G. Brauer, R.A. Yankov, V. Heera, M. Voelskow, R. Kögler, W. Skorupa, Radiation damage and annealing behaviour of Ge+-implanted SiC, Nucl. Instrum. Meth. Phys. Res. Sect. B Beam Interact. Mater. Atoms. 120 (1996) 177–180, https://doi.org/10.1016/S0168-583X(96)00504-6.